

Positively regulating the active sites to oxygen evolution reaction by *in situ* encapsulating NiFe₂O₄ nanoparticles in N-doped carbon nanotubes to construct efficient bifunctional oxygen catalyst for rechargeable Zn-air batteries

Yibo Tang^{a,1}, Ying Lei^{a,1}, Guijun Li^a, Tiantian Fu^a, Yang Xiang^a, Jingqi Sha^a, Hai Yang^a, Peng Yu^a, Yujun Si^{a,*}, Chaozhong Guo^{b,*}

^a College of Chemistry and Environmental Engineering, Sichuan University of Science and Engineering, Zigong 643000, China

^b College of Materials Science and Engineering, Chongqing University of Arts and Sciences, Chongqing 402160, China

1. UV-Vis diffuse reflectance spectra and FTIR spectra

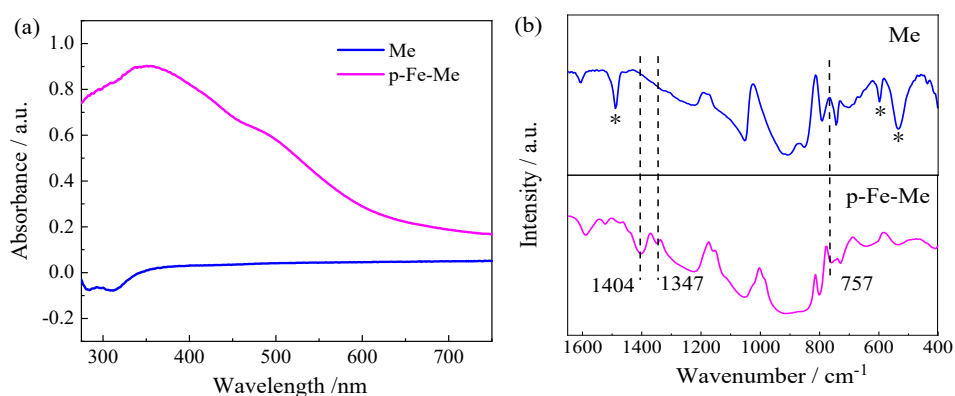


Figure S1 (a) UV-Vis diffuse reflectance spectra, (b) FTIR spectra of Melamine (Me) and precursor p-Fe-Me (“*” represents the weakened peaks).

2. Thermogravimetry analysis

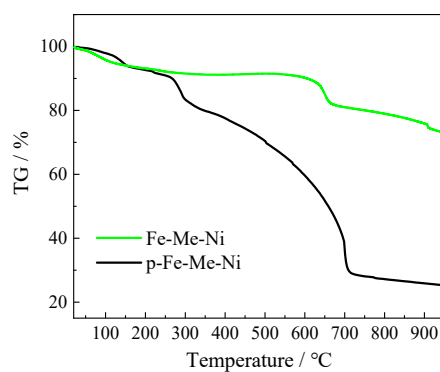


Figure S2 Thermogravimetry curves of Fe-Me-Ni and its precursor (p-Fe-Me-Ni).

3. RRDE measurement

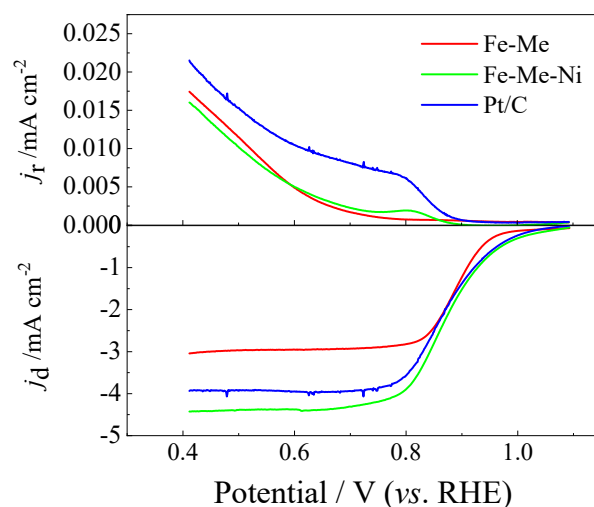


Figure S3 LSV curves on RRDE

4. Calculation of electrochemical active surface area (ECSA)

Cyclic voltammetry (CV) of catalyst was carried out in a potential range of 1.01~1.11 V (vs. RHE), at 2, 4, 6, 8, 10 and 12 mV s^{-1} of scan rate. Then a linear plot was drawn between the capacitive current densities at 1.06 V and the scan rate. The fitted slope of the plot represents the electrical double layer capacitance C_{dl} which can be employed to assess the electrochemical active surface area (ECSA). The higher C_{dl} corresponds to the greater ECSA.

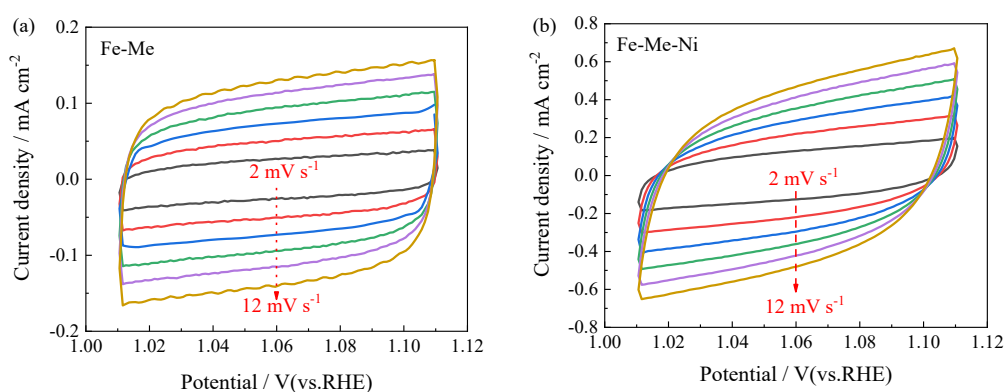


Figure S4 CV curves, (a) Fe-Me, (b) Fe-Me-Ni at various scan rates in 0.1 M KOH solution in a potential window without Faradaic current.

5. Galvanostatic discharge of Zn-air batteries

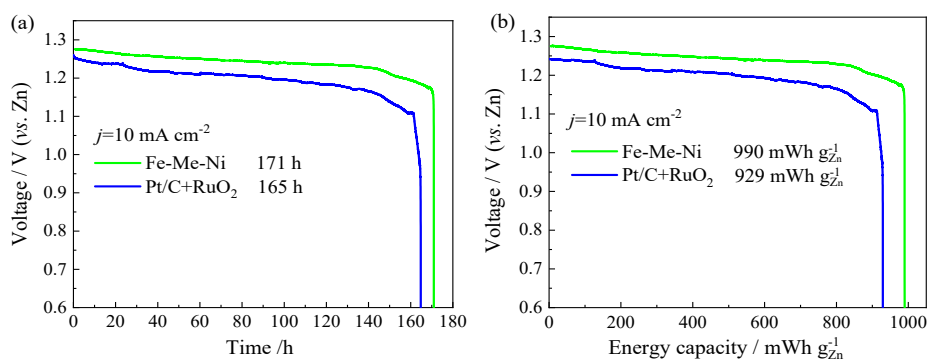


Figure S5 (a) Galvanostatic discharge curves of Zn-air batteries, (b) energy density of Zn-air batteries based on the loss of the Zn anode

6. Characterization of the aged Fe-Me-Ni

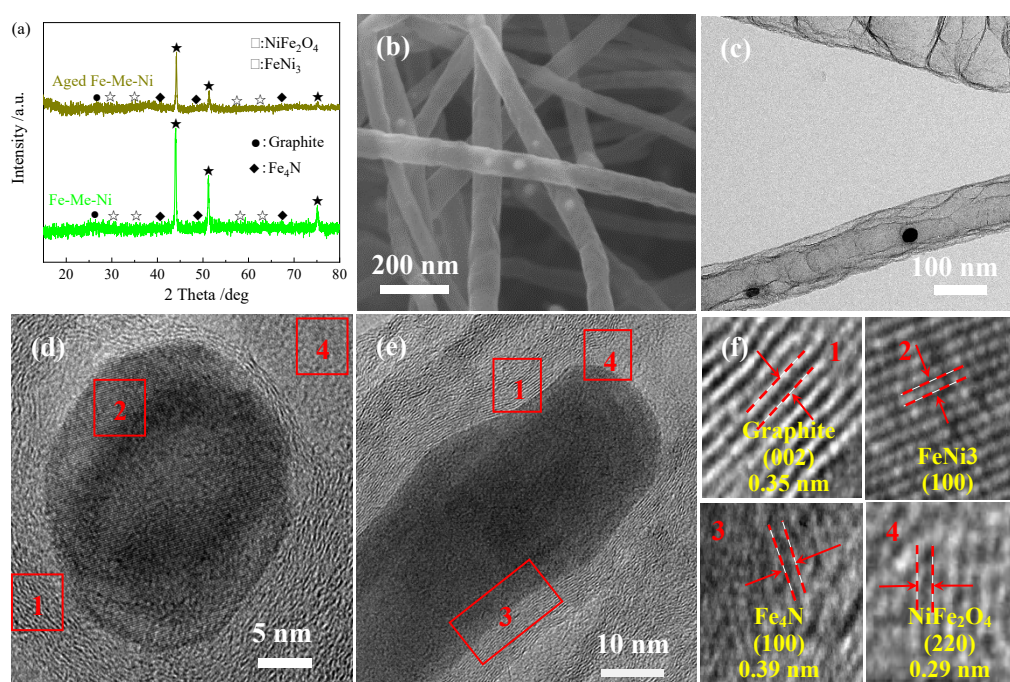


Figure S6 (a) XRD patterns of Fe-Me-Ni before and after aging experiment (Aged Fe-Me-Ni), (b) SEM image, (c) TEM image, (d, e) HRTEM images of the aged Fe-Me-Ni, (f) lattice fringes of graphite, FeNi₃, Fe₄N, and NiFe₂O₄ for region “1”, “2”, “3”, “4” circled in (d, e), respectively.

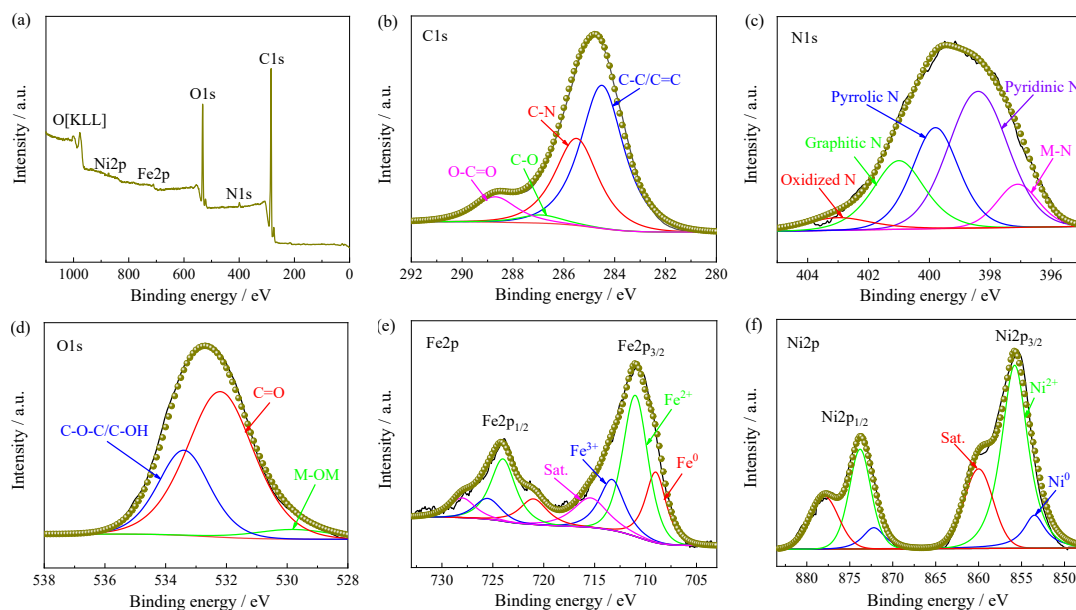


Figure S7 (a) XPS survey spectrum of aged catalyst Fe-Me-Ni, and the corresponding high-resolution XPS spectra of (b) C1s, (c) N1s, (d) O1s, (e) Fe2p, (f) Ni2p.

7. Comparison table on the catalytic performance of Fe-Me-Ni with references

Table S1 Comparison on the electrocatalytic activities of Fe-Me-Ni and performance of Zn-air batteries with recently reported bifunctional catalysts

Catalysts	ORR $E_{1/2}/V$	OER E_{10}/V	$\Delta E/V$	Specific capacity mAh g^{-1}	References
Fe-Me-Ni	0.841	1.543	0.702	798	This work
Co ₂ P@NCNTs-15	0.82	1.806	0.986	792.6	Ref. 1
FeNCFs	0.84	1.63	0.79	717	Ref. 2
Co-Co ₆ Mo ₆ C ₂ @NC	0.80	1.50	0.70	768	Ref. 3
Co ₃ W ₃ C/CoP/NPC	0.803	1.43	0.627	800.5	Ref. 4
Co@IC/MoC@PC	0.875	1.51	0.635	725	Ref. 5
CoNi/NHCS-TUC-3	0.88	1.686	0.806	756.5	Ref. 6
FeCo@NS-CA	0.85	1.68	0.83	760	Ref. 7
Co-UA-OCB	0.834	1.621	0.787	799	Ref. 8
CoFe/S-N-C	0.855	1.588	0.733	814	Ref. 9
FeCo-1/NSC	0.82	1.555	0.735	776	Ref. 10

References:

- (1) X. Peng, Y. Liu, S. Hu, P. Zheng, Y. Fu, P. Dong, J. Xiao, L. Han, Y. Zhang, Synthesis of a Highly Efficient Bifunctional $\text{Co}_2\text{P}@N$ -doped Carbon Nanotubes Electrocatalyst by GO-Induced Assembly Strategy for Rechargeable Zn-Air Batteries, *J. Alloys Compd.*, 2021, 889, 161628.
- (2) Y. Ma, D. Chen, D. Zhang, H. Yu, Y. Zheng, W. Li, L. Wang, Q. Liu, W. Yang, Fe,N-Modulated Carbon Fibers Aerogel as Freestanding Cathode Catalyst for Rechargeable Zn-Air Battery, *Carbon*, 2022, 187, 196-206.
- (3) S. Chen, X. Liu, H. Sun, Z. Cao, J. Xiong, Y. Li, Facile Synthesis of Carbon Coated Cobalt-cobalt Molybdenum Carbide as Advanced Bifunctional Oxygen Electrocatalyst for Rechargeable Zn-Air Battery, *J. Alloys Compd.*, 2022, 897, 163203.
- (4) Y. Zhang, W. Shi, L. Bo, Y. Shen, X. Ji, L. Xia, X. Guan, Y. Wang, J. Tong, Electrospinning Construction of Heterostructural $\text{Co}_3\text{W}_3\text{C}/\text{CoP}$ Nanoparticles Embedded in N,P-doped Hierarchically Porous Carbon Fibers as Excellent Multifunctional Electrocatalyst for Zn-Air Batteries and Water Splitting, *Chem. Eng. J.*, 2022, 431, 134188.
- (5) L. Zhang, Y. Zhu, Z. Nie, Z. Li, Y. Ye, L. Li, J. Hong, Z. Bi, Y. Zhou, G. Hu Co/MoC Nanoparticles Embedded in Carbon Nanoboxes as Robust Trifunctional Electrocatalysts for a Zn-Air Battery and Water Electrocatalysis, *ACS Nano*, 2021, 15, 13399-13414.
- (6) K. Sheng, Q. Yi, A.L. Chen, Y. Wang, Y. Yan, H. Nie, X. Zhou, CoNi

Nanoparticles Supported on N-Doped Bifunctional Hollow Carbon Composites as High-Performance ORR/OER Catalysts for Rechargeable Zn-Air Batteries, *ACS Appl. Mater. Interfaces*, 2021, 13, 45394-45405.

(7) H. Pang, P. Sun, H. Gong, N. Zhang, J. Cao, R. Zhang, M. Luo, Y. Li, G. Sun, Y. Li, J. Deng, M. Gao, M. Wang, B. Kong, Wood-Derived Bimetallic and Heteroatomic Hierarchically Porous Carbon Aerogel for Rechargeable Flow Zn-Air Batteries, *ACS Appl. Mater. Interfaces*, 2021, 13, 39458-39469.

(8) T. Fu, G. Li, Y. Xiang, Y. Tang, D. Cai, S. Jiang, Y. Xue, Z. Xiong, Y. Si, C. Guo, Hierarchical Cobalt-Nitrogen-Doped Carbon Composite as Efficiently Bifunctional Oxygen Electrocatalyst for Rechargeable Zn-Air batteries, *J. Alloys Compd.*, 2021, 878, 160349.

(9) G. Li, Y. Tang, T. Fu, Y. Xiang, Z. Xiong, Y. Si, C. Guo, Z. Jiang, S, N Co-doped Carbon Nanotubes Coupled with CoFe Nanoparticles as an Efficient Bifunctional ORR/OER Electrocatalyst for Rechargeable Zn-air Batteries. *Chem. Eng. J.*, 2022, 429, 132174.

(10) S. Chang, H. Zhang, Z. Zhang, FeCo Alloy/N, S Dual-Doped Carbon Composite as a High-Performance Bifunctional Catalyst in an Advanced Rechargeable Zinc-Air Battery, *J. Energy Chem.*, 2021, 56, 64-71.